A 3D Wide Passband Frequency Selective Surface with Sharp Roll-off Sidebands and Angular Stability

Wang, Peng; Jiang, Wen ; Hong, Tong ; Li, Yunfeng; Shen, Ming; Pedersen, Gert Frølund

Published in:
I E E E Antennas and Wireless Propagation Letters

DOI (link to publication from Publisher):
10.1109/LAWP.2021.3126890

Publication date:
2022

Document Version
Accepted author manuscript, peer reviewed version

This article has been accepted for publication in a future issue of this journal, but has not been fully edited. Content may change prior to final publication. Citation information: DOI 10.1109/LAWP.2021.3126890, IEEE Antennas and Wireless Propagation Letters

A 3D Wide Passband Frequency Selective Surface with Sharp Roll-off Sidebands and Angular Stability

Peng Wang[1], Wen Jiang[1], *Member, IEEE*, Tao Hong[1], *Member, IEEE*,

Yunfeng Li[2], *Student Member, IEEE*, Gert F. Pedersen[2], and Ming Shen[2], *Member, IEEE*.

***Abstract*— In this letter, a 3D wide passband frequency selective surface (FSS) is proposed. Compared with planar wide passband FSSs, 3D structures usually present superior roll-off characteristics, especially under lower frequency. However, 3D wideband FSSs typically have greater insertion loss in the passband, and the transmission characteristic is sensitive to the angle of incident electromagnetic wave. The proposed FSS, by concurrently applying the design methods of planar FSSs and 3D FSSs, provides sharp double roll-off sidebands while maintaining excellent angular stability and low insertion loss in a wide passband. The simulation results show that the designed FSS can achieve a passband range from 5.86 GHz to 13.4 GHz with an insertion loss of less than 1 dB, and it can retain a stable transmission characteristic with the incident angle ranging from 0° to 45°. The proposed FSS is fabricated and measured in an anechoic chamber, and the measured results show that the fabricated FSS achieves a -3 dB passband from 5.33 GHz to 14.5 GHz. Under different incident angles ranging from 0° to 45°, the FSS also features the lower and upper roll-off transition bandwidths of 6.4% and 4.7%, respectively.**

***Index Terms*— Frequency Selective Surface; 3D Structure; Wideband; Double Roll-off Sidebands; Angular Stability.**

I. INTRODUCTION

FREQUENCY selective surface (FSS) is a periodic structure, which realizes the transmission and reflection of space electromagnetic waves in specific frequency bands [1]. It is widely used in radomes, antenna reflectors, electromagnetic shielding, etc. [2-4]. In 5G and 6G, FSSs will be widely used in more communication fields [5, 6].

In recent years, broadband communication systems put forward more stringent bandwidth requirements [7-9]. Wide passband FSSs can realize the transmission of electromagnetic waves in a wide band with low insertion loss. The design of wide passband FSS has been previously studied by several works [10-16]. In [10], a planar ultra-wideband FSS unit cell is presented with three layers of patches. Planar wide passband FSSs are also implemented with other technologies like absorbers [11], miniaturization technologies [12, 13] and so on. However, all these planar wideband FSSs share a common drawback: it is sophisticated to attain high suppression at lower frequency to avoid interferences. Some works tried to deal with this issue, but they lead to a narrowed passband and show insignificant improvement [14-16].

3D wide passband FSSs can realize double roll-off sidebands [17-20]. In [17], a roll-off sidebands 3D wide passband FSS is presented with sharp roll-off sidebands. In [18], a 3D wide passband FSS with a stacked slot-line is presented. In [19], a 3D ultra-wideband bandpass FSS is designed with sub-wavelength staggered metallic frames.

However, the insertion loss of 3D FSSs is greater than planar structures. Compared to existing wide passband FSSs, planar structures can easily achieve wide passband within 1-dB insertion loss, but the insertion loss of 3D structures is out of 1-dB. Besides, 3D FSSs are also sensitive to the variation of incident wave angles due to the high profile. Therefore, they can only maintain the response within a narrow range of incident angles. The structure in [19] can achieve angular stability ranging from 0° to 30° with only simulation results. Moreover, most 3D wide passband FSSs only show satisfactory performance when incident electromagnetic waves radiate vertically on their surfaces [17, 18].

In this paper, combining planar FSSs and 3D FSSs, a 3D wide passband FSS is proposed. The transition bands of the structure at the lower and upper edge of the passband are 4.9% and 1.8%, respectively. The simulation results exhibit attractive characteristics of double roll-off sidebands, low insertion, and stable performance. The FSS is fabricated and measured in a microwave anechoic chamber. The measured results show a satisfactory –3 dB bandwidth from 5.33 GHz to 14.5 GHz with the angular stability ranging from 0° to 45°. The measured transition bands are 6.4% and 4.7%, respectively.

II. FSS ELEMENT DESIGN

A. FSS Configuration

Based on models in ref [10] and ref [17], the proposed FSS comprises two layers of metallic grids and two cascaded triangular-shaped elements connected via four vertical wires as shown in Fig.1. Fig. 1(a) is the 3D view of the FSS array. Figs. 1(b) and 1(c) are the 3D views of the FSS unit element, and Fig. 1(d) shows the triangular-shaped metallic rings printed on the upper dielectric substrate, which are connected to bottom triangular-shaped metallic rings via four vertical wires. Fig. 1(e) exhibits the metallic grid and two groups of resonant square rings. The relative permittivity of each dielectric substrate in design FSS is 2.2, and the loss tangent is 0.002.

Manuscript received XXXX. This work was supported by the National Natural Science Foundation of China under grant 62071347.

Peng Wang, Wen Jiang and Tong Hong are with the National Key Laboratory of Antennas and Microwave Technology, Xidian University, Xi'an, Shaanxi, 710071, China.(e-mail: pengwang0308@gmail.com; jw13@vip.qq.com).

Yunfeng Li, Gert F. Pedersen, and Ming Shen are with the Department of Electronic Systems, Aalborg University, 9220, Aalborg, Denmark.

Color versions of one or more of figures in this communication are available online at http://ieeexplore.ieee.org.

Digital Object Identifier xxxxxxxxxx

This article has been accepted for publication in a future issue of this journal, but has not been fully edited. Content may change prior to final publication. Citation information: DOI 10.1109/LAWP.2021.3126890, IEEE Antennas and Wireless Propagation Letters

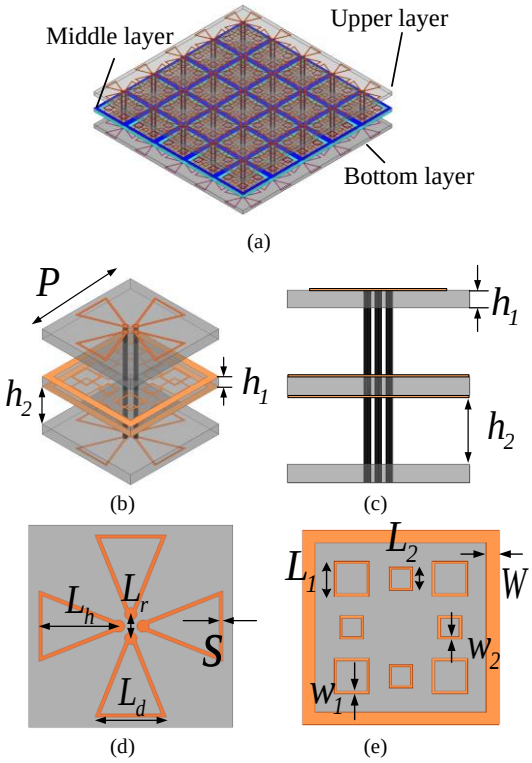

Fig. 1. Geometry of the proposed wideband FSS. (a) 3-D view of the array surface. (b) 3-D view of the FSS element. (c) Side view of the FSS element. (d) Upper layer of the triangular-shaped elements. (e) Middle layer of the metallic grid and two groups of resonant metallic rings.(unit: mm, P=10, L_h=3.9, L_d=3.5, S=0.16, W=0.65, L_r=1.2, L_1=1.8, w_1=0.12, L_2=1.2, w_2=0.12, h_1=1, and h_2=3.7).

Two layers of metallic grids are printed on a dielectric substrate, which helps build the stopband in lower frequency ranges, functioning as inductances. Two groups of resonant metallic rings are designed in the metallic grid to improve angular stability. Moreover, two cascaded elements connected via the vertical wires realize the stopband in the upper frequency range. Vertical wires connecting two layers of metallic patches also increase the size of the resonant structure and realize roll-off stopband. Air layers between dielectric substrates avoid the coupling between metallic patches.

Some parameters are simply analysis as follow, L_h influences the coupling between elements, so the value of L_h is more carefully designed. The parameters of dielectric substrate have a great influence on performance due to impedance matching. Besides, reducing the value of h_2 will reduce the size of resonant structure and increase the resonant frequency.

B. *Analysis of Current Distributions*

The current distribution of the FSS is shown in Fig. 2 when the E-field of the incident wave is horizontally polarized. Fig. 2(a) demonstrates the current distribution at 3 GHz. It shows that the current is mainly located in the metallic grid in the y-axis direction, which means the metallic grid affects the transmission of the electromagnetic wave in lower frequency and achieves stopband. Fig. 2(b) shows the current distribution in the bandpass at 10 GHz, and there is no area with dense current distribution, which means the electromagnetic wave passes through the FSS with low insertion loss. Fig. 2(c) shows the current distribution at 17 GHz. The major part of current is located in triangular-shaped rings in the y-axis direction, indicating that the connected triangular-shaped rings resonate and achieve the stopband in upper frequency.

Fig. 2(d) is the current distribution of two different middle layers under 45 ° incidence angle of the electromagnetic wave in upper frequency at 17 GHz. The upper figure shows the metallic grid without resonator rings, and the bottom one is with resonator rings. It can be seen that the current is distributed on the resonator rings with large magnitude values. It means the small resonator rings play an important role in blocking the transmission of electromagnetic waves.

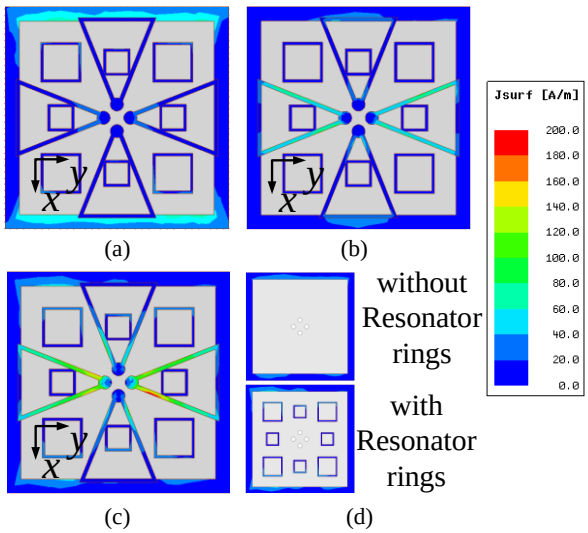

Fig. 2. Current distribution of FSS. (a) Stopband at 3 GHz (b) Passband at 10 GHz (c) Stopband at 17 GHz (d) Middle layer under 45° incidence angle of electromagnetic wave (17 GHz).

C. *Equivalent Circuit Modeling and Analysis*

The designed FSS circuit model of the is shown in Fig. 3. In the series LC resonant circuit, the quality factor Q is calculated as:

$$Q=\frac{1}{R}\sqrt{\frac{L}{C}}. \quad (1)$$

The bandwidth of the stopband resonance becomes narrower as the quality factor increases, and the transition bandwidth will decrease consequently, which can be used to realize sharp roll-off sidebands. Fig. 3(a) is formed as a resonator by oppositely connecting the triangular-shaped elements. In this structure, the triangular metallic rings can equip with inductance L_{11}, L_{12}, L_{21}, and L_{22}. C_{u1} and C_{d1} are coupling capacitance between triangular metallic rings; C_{u2} and C_{d2} represent the coupling capacitance between elements; L_1 and L_2 are the equivalent inductances of the metallic vertical wires; C_{12} is the coupling capacitance between metallic vertical wires. Fig. 3(b) is equivalent to two layers of inductance paralleled connected with series LC. The metallic grips are equivalent to inductance L_a and L_b, which realize the stopband in lower frequency. The two sets of metallic rings can simply equip with a series resonant LC. The equivalent circuit of the proposed FSS is shown in Fig. 3(c).

This article has been accepted for publication in a future issue of this journal, but has not been fully edited. Content may change prior to final publication. Citation information: DOI 10.1109/LAWP.2021.3126890, IEEE Antennas and Wireless Propagation Letters

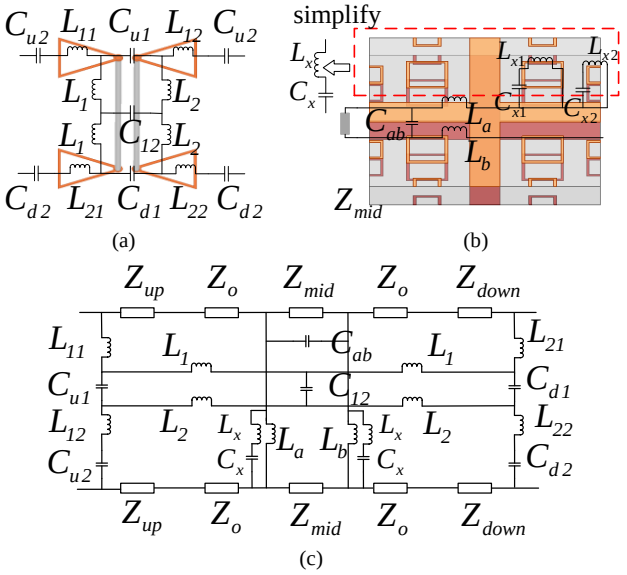

Fig. 3. Equivalent circuit model of (a) the connected triangular-shaped element, (b) the middle layer, and (c) the FSS.

TABLE I
VALUES OF THE COMPONENTS IN THE EQUIVALENT CIRCUIT MODEL

Parameter	L_{11}	L_{12}	L_{21}	L_{22}	C_{u1}	C_{u2}	C_{d1}	C_{d2}
Value	0.47	0.24	0.34	0.43	0.07	0.05	0.07	0.04
Parameter	C_{12}	L_1	L_2	L_a	L_b	C_{ab}	L_x	C_x
Value	0.02	7.43	5.13	0.65	0.5	0.02	0.29	0.03

*The units of inductance and capacitance are nH and pF respectively.

The values of equivalent capacitance and inductance in Fig. 3 are calculated by ADS [21-23], as shown in Table I. The comparision of equivalent circuit simulation by ADS and fullwave electromagnetic simulation by HFSS are presented in Fig. 4, which demonstrates a satisfactory consistency.

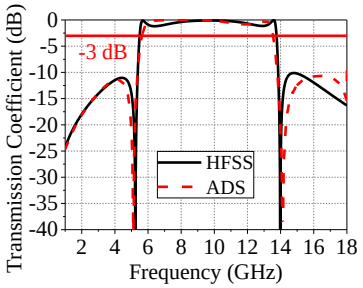

Fig. 4. The comparison of ADS and HFSS simulation results.

III SIMULATION AND MEASUREMENT

A. Simulation

The transmission curves of the designed FSS and component elements are shown in Fig. 5. Fig. 5(a) presents the transmission curves of connected triangular-shaped elements. Fig. 5(b) shows the transmission curves of metallic grids with and without resonant rings at the 45 ° incident angle.

Fig. 5(c) illustrates the transmission curves of FSS without two groups of resonant square rings. It presents a wide passband with low insertion loss and double roll-off sidebands. However, its performance varies drastically with different

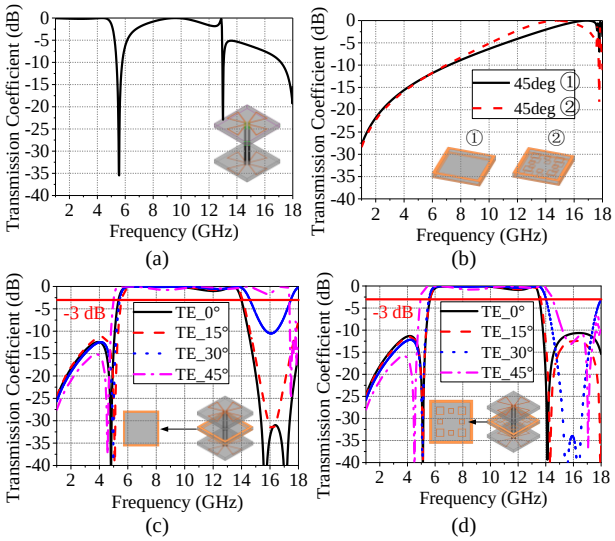

Fig. 5. Simulated transmission curves of (a) the structure of connected triangular-shaped elements, (b) the structure of metallic grids with resonant square rings and without resonant square rings, (c) the designed FSS without resonant rings, and (d) the designed FSS with resonant rings (final structure).

incident angles of the signal. To improve the angular stability, the final FSS is designed, and the simulation results are shown in Fig. 5(d). The final FSS achieves a –1 dB bandwidth from 5.86 GHz to 13.4GHz. Moreover, the upper and lower transition bands are 4.9% and 1.8%, respectively. Furthermore, the structure shows clear stability under different incident angles (up to 45°) of electromagnetic waves.

B. Fabrication and Measurement

The final FSS design was fabricated, and the fabricated process is shown in Fig.6(a). Firstly, using plastic columns to fix the dielectric substrate. Then, let the plastic screw pass through nonmetallic vias and plastic columns, and the plastic nut fixes the plastic screw. Then, let vertical wires pass through metallic vias and fixing the structure with the help of foam, electric iron, and solder. Finally, flipping the structure and fixing the other side. The prototype is shown in Fig. 6(b) and Fig. 6(c).

The measurement setup of the fabricated prototype is shown in Fig. 7. The prototype is placed in the middle of two horn antennas. One horn antenna is used to emit electromagnetic waves, while the other one is to receive electromagnetic waves. The antennas are connected to a vector network analyzer (VNA) to measure the transmission coefficients of the prototype. The FSS is surrounded by absorber screens to suppress the diffraction.

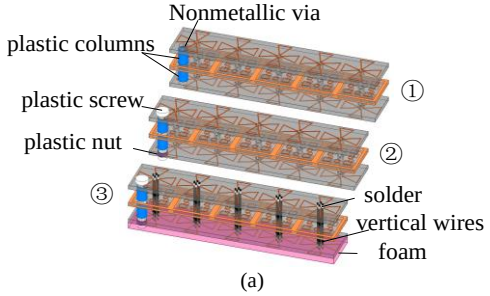

This article has been accepted for publication in a future issue of this journal, but has not been fully edited. Content may change prior to final publication. Citation information: DOI 10.1109/LAWP.2021.3126890, IEEE Antennas and Wireless Propagation Letters

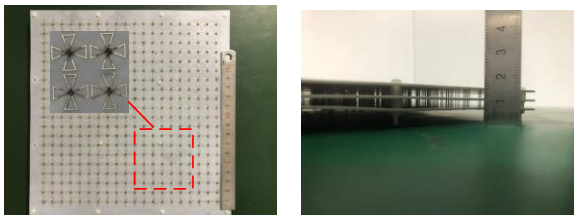

(b) (c)

Fig. 6. The fabricated FSS. (a) Processing process (b) Top-view. (c) Side view.

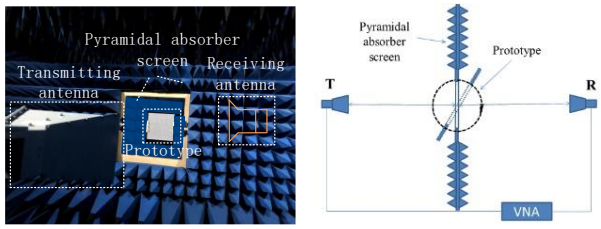

(a) (b)

Fig. 7. Demonstration of the measurement setup. (a) Setup under test (transmitting side). (b) Measurement diagram.

The measured results are shown in Fig. 8(a). When the prototype surface is perpendicular to the main beams of the two horn antennas, the incident angle of the electromagnetic wave is 0°. In this case, the prototype achieves a wideband transmission from 5.33 GHz to 14.5 GHz with an insertion loss less than 3 dB. The stopbands with insertion loss larger than 10 dB are from 1 GHz to 5 GHz and 15.2 GHz to 18 GHz. The transition bands of the prototype are 6.6% in the lower band and 4.7% in the upper band, respectively. Furthermore, the prototype features stable transmission characteristics within a broad incidence angle ranging from 0° to 45°.

Here are some possible reasons to explain why the measured results are somewhat different from the original simulation. Firstly, the prototype presents a slight difference from the simulation structure as follows. The actual length of metallic wires is longer than the design for welding, which will increase the insertion loss in the passband. Plastic columns fix the two air layers between three dielectric substrates. The actual height of the air layers is smaller than simulation, which will reduce the size of the structure and makes stopband in higher frequency. After changing those parameters and the simulation results are shown in Fig. 8(b). Besides, the inhomogeneous distribution of the dielectric constant of the dielectric substrate will also influence transmission characteristics.

The overall size of the prototype is 210 mm×210 mm. The relatively small electrical dimension of the prototype has an impact on the measurement accuracy in lower frequency.

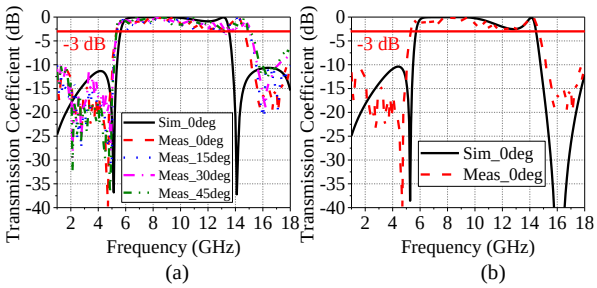

(a) (b)

Fig. 8. Measurement and simulation results of the TE model. (a) The simulation results and measurement results. (b) The simulation results of actual prototype and measurement results.

Hence, the measured results and simulation results do not match well below 2.5 GHz. Nevertheless, in overall the measured results are in good agreement with simulation results.

The performance comparison of the proposed FSS and previous wide passband FSSs are shown in Table II.

TABLE II
PERFORMANCE COMPARISON WITH RESPECT TO PREVIOUS WORKS

Ref	Type	Passband (3-dB)	Lower and upper roll-off bandwidth	Angular stability	Element Size (λ)
[10]	2D	105% (Meas)	45% & 10.5%	30°	0.12
[16]	2D	63% (Meas)	12.5% & 3.8%	40°	0.22
[17]	3D	65% (Meas)	4.2% & 1.4%	NA	0.14
[18]*	3D	75% (Sim)	NA & 9.7%	NA	0.08×0.13
[19]*	3D	100% (Sim)	8.3% & 1%	30°	0.128
[20]*	3D	67% (Sim)	11.8% & NA	NA	0.27
This Work	3D	78.5%(Sim)	4.9%&1.8%	45°	0.17
		92.5% (Meas)	6.4% & 4.7%		

*The lower and upper roll-off bandwidth is the transition bandwidth where S21 varies between – 10 dB and -3 dB.

It is worth pointing out that [10] and [16] are planar wide passband FSSs, which show good angular stabilities for oblique incident angles up to 40°. However, their roll-off bands are wide, especially in lower frequency. Compared with the planar structure, the designs in [17]-[20] are 3D wide passband FSSs. These structures present good roll-off sidebands. However, the characteristics of 3D structures are sensitive to the angle of the incident electromagnetic wave due to the high profile. Furthermore, most of these 3D FSSs are only simulated without experimental validation due to the complex structures.

The proposed FSS combines the design methods of 3D and planar wide passband FSSs. It achieves the high angular stability (up to 45°) and sharp roll-off characteristics (lower than 7%) simultaneously. The measured results also show that it realizes a 3-dB passband bandwidth from 5.33 GHz to 14.5 GHz. This is achieved while maintaining stable characteristics ranging from 0° to 45° incident angles. Meanwhile, the double roll-off sidebands in the lower and upper frequency bands achieve 6.4% and 4.7% transition bandwidths, respectively.

IV CONCLUSION

In this letter, a 3D wide passband frequency selective surface (FSS) with sharp double roll-off sidebands, angular stability, and low insertion loss is proposed. The FSS is achieved by concurrently applying the design methods of 3D and planar wide passband FSSs. Both simulations and measurements validate the proposed FSS. Measured results show a wide bandwidth from 5.33 GHz to 14.5 GHz, while double roll-off sidebands with transition bandwidths of 6.4% and 4.7% are achieved in lower frequency and upper frequency, respectively. Compared with existing 3D wide passband FSSs, the designed 3D FSS is straightforward to fabricate and delivers a novel method to improve the angular stability (up to 45°), which can also be used to deal with the issues of resonance weakening in oblique incident angles.

REFERENCES

[1] C. Zhao, C. Wang and S. Aditya, "Power-dependent frequency-selective surface: concept, design, and experiment," *IEEE Trans. Antennas Propag.*, vol. 67, no. 5, pp. 3215-3220, May 2019.

[2] P. -S. Wei, C. -N. Chiu, C. -C. Chou and T. -L. Wu, "Miniaturized dual-band FSS suitable for curved surface application," *IEEE Antennas Wireless Propag. Lett.*, vol. 19, no. 12, pp. 2265-2269, 2020.

[3] L. Kurra, M. P. Abegaonkar, A. Basu and S. K. Koul, "FSS properties of a uniplanar EBG and its application in directivity enhancement of a microstrip antenna," *IEEE Antennas Wireless Propag. Lett.*, vol. 15, pp. 1606-1609, 2016.

[4] R. Sivasamy, B. Moorthy, M. Kanagasabai, V. R. Samsingh and M. G. N. Alsath, "A wideband frequency tunable FSS for electromagnetic shielding applications," *IEEE Trans. Electromagn. Compat*., vol. 60, no. 1, pp. 280-283, Feb. 2018.

[5] M. Borhani Kakhki, A. Dadgarpour, A.-R. Sebak, and T. A. Denidni, "Twenty-eight-gigahertz beam-switching ridge gap dielectric resonator antenna based on FSS for 5G applications," *IET Microw., Antennas Propag*., vol. 14, no. 5, pp. 397–401, Apr. 2020.

[6] D. Li et al., "A low-profile broadband bandpass frequency selective surface with two rapid band edges for 5G near-field applications," *IEEE Trans. Electromagn. Compat*., vol. 59, no. 2, pp. 670-676, Apr. 2017.

[7] R. Xu, J. Li, K. Wei and G. Yang, "A broadband slot antenna with unidirectional circularly polarized radiation patterns," *IEEE Antennas Wireless Propag. Lett.*, vol. 16, pp. 317-320, 2017.

[8] H. Son, T. Jang, S. Kim, K. Jung, J. Kim and C. Park, "Pole-controlled wideband 120 GHz CMOS power amplifier for wireless chip-to-chip communication in 40-nm CMOS process," *IEEE Trans. Circuits Syst. II Exp. Briefs*, vol. 66, no. 8, pp. 1351-1355, Aug. 2019.

[9] X. Zhong, H.-X. Xu, L. Chen, W. Li, H. Wang, and X. W. Shi, "An FSS-backed broadband phase-shifting surface array with multimode operation," *IEEE Trans. Antennas Propag*., vol. 67, no. 9, pp. 5974–5989, Sep. 2019.

[10] H. Zhou et al., "Ultra-wideband frequency selective surface," *Electron. Lett*., vol. 7, no. 1, pp. 11–13, Jan. 2012.

[11] Q. Chen, D. Sang, M. Guo and Y. Fu, "Miniaturized frequency-selective rasorber with a wide transmission band using circular spiral resonator," *IEEE Trans. Antennas Propag.*, vol. 67, no. 2, pp. 1045-1052, Feb. 2019.

[12] R. S. Anwar, Y. Wei and H. S. Ning, "A broadband third-order antenna-filter-antenna based frequency selective surface at high oblique angle of incidence," *2017 Progress in Electromagnetics Research Symposium - Fall (PIERS - FALL)*, pp. 513-518, 2017.

[13] Y. Cui, S. Zhang and M. Wang, "A triple-layer frequency selective surface with flat wide passband," *2019 IEEE International Conference on Computational Electromagnetics (ICCEM)*, pp. 1-3, 2019.

[14] D. Feng, Z. Shenquan, D. Fan, and W. Dongdong, "A n-order ultra wideband frequency selective surface," *Proc. Int. Symp. Antennas, Propag. Em Theory*, pp. 648–651, Oct. 2016.

[15] D. Li, T.-W. Li, R. Hao, H.-S. Chen, W.-Y. Yin, H.-C. Yu, et al., "A low-profile broadband bandpass frequency selective surface with two rapid band edges for 5G near-field applications," *IEEE Trans. Electromagn. Compat.*, vol. 59, no. 2, pp. 670-676, Apr. 2017.

[16] Q. Lv, C. Jin, B. Zhang and R. Mittra, "Wide-passband dual-polarized elliptic frequency selective surface," *IEEE Access*, vol. 7, pp. 55833-55840, 2019.

[17] C. Pelletti, G. Bianconi, R. Mittra and Z. Shen, "Frequency selective surface with wideband quasi-elliptic bandpass response," *Electron. Lett.*, vol. 49, no. 17, pp. 1052-1053, Aug. 2013.

[18] B. Li et al. "Wideband frequency selective structures based on stacked microstrip/slot lines," *2018 International Conference on Microwave and Millimeter Wave Technology (ICMMT)*, pp.1-3, 2018.

[19] Hu, Wenxiu, et al. "3D ultra-wideband high selective bandpass FSS," *2019 IEEE MTT-S International Wireless Symposium (IWS)*, pp.1-3, 2019.

[20] Y. Zhao, J. Fu, Z. Liang, Z. Zhang, Z. Wang, K. Zhang, et al., "A novel ultra-wideband switch-type active frequency selective surface for radome applications," *Proc. 13th Eur. Conf. Antennas Propag. (EuCAP)*, pp. 1-4, Mar. 2019.

[21] N. Liu, X. Sheng, C. Zhang, J. Fan and D. Guo, "A Design Method for Synthesizing Wideband Band-Stop FSS via Its Equivalent Circuit Model," *IEEE Antennas Wireless Propag. Lett.*, vol. 16, pp. 2721-2725, 2017.

[22] T. Hong, K. Peng and M. Wang, "Miniaturized Frequency Selective Surface Using Handshake Convoluted Stripe," *IEEE Antennas Wireless Propag. Lett.*, vol. 18, no. 10, pp. 2026-2030, 2019.

[23] S. S. Bukhari, W. G. Whittow, J. C. Vardaxoglou and S. Maci, "Equivalent Circuit Model for Coupled Complementary Metasurfaces," *IEEE Trans. Antennas Propag.*, vol. 66, no. 10, pp. 5308-5317, Oct. 2018.